Volume 19
Number 2

December *2017*
(ISSN 1109-1606)

Journal of

APPLIED ELECTROMAGNETISM

JAE

Institute of Communication and Computer Systems

Athens - GREECE

Volume 19 **December 2017**
Number 2 **(ISSN 1109-1606)**

JOURNAL
OF
APPLIED ELECTROMAGNETISM

Institute of Communication and Computer Systems

Athens - GREECE

Volume 19 **Number 2**

December 2017

TRANS BLACK SEA REGION UNION OF APPLIED ELECTROMAGNETISM (BSUAE)

JOURNAL OF APPLIED ELECTROMAGNETISM

Institute of Communication and Computer Systems

Athens - GREECE

Publishing Department

Journal of Applied Electromagnetism

Copyright Form

The undersigned I confirm that I agree the publication of the article

in the Journal of Applied Electromagnetism and the copyright to belong to Trans Black Sea Union of Applied Electromagnetism. I understand that I have the full right to reuse this manuscript for my own purposes.

Name:

Surname:

Address:

E-mail:

Signed:

***Please send the previous form signed either by e-mail to pfrangos@central.ntua.gr , or by fax to the fax number: +30 210 772 2281, attention of Prof. P. Frangos.**

Address

Institute of Communication and Computer Systems,

National Technical University of Athens,

9, Iroon Polytechniou Str.,

157 73 Athens - GREECE

Tel: (+30) 210 772 3694

Fax: (+30) 210 772 2281, attention of Prof. P. Frangos

e-mail: pfrangos@central.ntua.gr

Web site: **http://jae.ece.ntua.gr**

TRANS BLACK SEA REGION UNION OF APPLIED ELECTROMAGNETISM (BSUAE)

JOURNAL OF APPLIED ELECTROMAGNETISM (JAE)

Volume 19 Number 2 December 2017

CONTENTS

path loss between the transmitter and the receiver is getting raised due to various external factors (conditions) that appear on weather. The characteristics of optical wireless systems and it changes in the face of different weather conditions strongly affect the parameters of Quality of Service. Also, this influence provides the possibility to quantify the significance of the service disruption impact to the metrics of Quality of Experience. Due to this, this paper gives a new approach to the relation of the characteristics of optical wireless communication system, known as Free Space Optics, affected during the weather-based disruptions with the parameters of Quality of Service. Furthermore, this relation is used in estimation of Quality of Experience metrics.

MULTIFUNCTIONAL ADAPTIVE SYSTEM FOR PHYSIOTHERAPY (selected from CEMA'17 Conference)

A. Dimitrov, S. Guergov, D. Dimitrov **33**

An investigation on structure of one multifunctional adaptive system for physiotherapy with measurement devices has been done in the paper. In the paper there are descriptions of different parts of the multifunctional system. Some characteristics and properties of different units of multifunctional system have been done, also. Some possibilities for simultaneously applications of different system's units are described, also. It's important to provide simultaneously application of different system's units only when their physiological influences on the human body are compatible. Simultaneously application of magneto-therapy, mechanical acupressure and cranial electro stimulation are described in the paper.

DIFFRACTION OF A PLANE EM WAVE FROM AN INFINITELY THIN PERFECTLY CONDUCTING RECTANGULAR PLATE (short paper)

K. Kotetishvili, G. Kevanishvili, I. Kevanishvili, G. Chikhladze

Georgian Technical University (GTU)

0175, 77, M. Kostava str., Tbilisi, Georgia

E-mail: ketinooo@hotmail.com, irakli1966@gmail.com, gurchix@gmail.com

Abstract

This paper deals with the problem of diffraction of a plane electromagnetic (EM) wave from a perfectly conducting rectangular plate at normal incidence. For the surface current arising on the plate two-dimensional integral equation is derived, which is solved approximately, using the method of δ-like functions. The calculating formula for the radiation characteristic of the plate is received and the corresponding radiation patterns are built.

1. INTRODUCTION AND PROBLEM FORMULATION

The problem of diffraction of a plane EM wave at extremely thin ideally conducting rectangular plate as far, as we know, is not yet considered in the scientific literature as the boundary problem of the mathematical physics, while its cognitive and practical value is too high. The cognitive value relates to the necessity of application of an original mathematical approach to its solution, while its practical application could be seen in SHF and antenna techniques. In figure the orientation of the plate in rectangular (X, Y, Z) reference frame is presented, but in future we shall use the spherical reference frame (R, θ, φ) as well.

Assume δ - thickness of the plate to be extremely small, and the origin of the reference frame to be selected in its center.

Assume now the plane, *E*-polarized *EM* wave incidents at the plate from right-hand side (X > 0), having only vertical E_z component of the electric field (see Fig. 1):

$$E_z = E_0 e^{ikx+i\omega t} \tag{1}$$

$E_{0,}$ being the given amplitude, while $k = {}^{2\pi}/_{\lambda}$, λ –the wavelength in vacuum, and ω the circular frequency of the field (further, $e^{i\omega t}$ time multiplier will be suppressed) [1].
The electric field strength E_{1z} in the wave, reflected from the plate is presented in the standard way:

$$E_{1z} = k^2 \Pi_{1z} + \frac{\partial^2 \Pi_{1z}}{\partial z^2} \tag{2}$$

Here Π_{1z} is Hertz's function given as follows:

$$\Pi_{1z} = C \int_{-a/2}^{a/2} \int_{-b/2}^{b/2} J(y', z') \frac{e^{-ikr}}{r} dy' dz' \tag{3}$$

with $C = {}^{1}/_{4\pi i \omega \varepsilon_0}$, a, b –the width and the height of the plate respectively and

$$\varepsilon_0 = {}^{1}/_{36\pi} \cdot 10^{-9} \left(\frac{F}{m}\right), \tag{4a}$$

$$r = \sqrt{x^2 + (y - y')^2 + (z - z')^2} \tag{4b}$$

$x, y, z -$ coordinates of M point of observation outside the plate, while y', z' are the transverse and vertical coordinates of M' point arbitrary selected at the plate, and r being the distance between M and M' points. $J(y', z')$is the current density arising at the surface of the plate, being the source of E_{1z} field scattered by the plate [2].

Our problem consists in the determination of the structure of the scattered E_{1z} field in any arbitrary point M of space, as the function of x, y, z coordinates, satisfying zero boundary conditions:

$$E_{1z'} + E_{2z''} = 0, \tag{5}$$

at the surface of the plate, when $x = \delta, y = y''$, $z=z''$, z', z'' being the coordinates of arbitrary M" point at the surface of the plate.

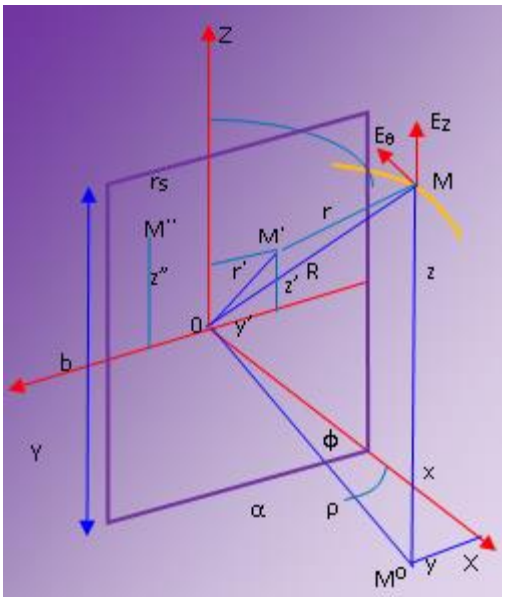

Figure 1. Diffraction of plane EM wave at an extremely thin ideally conducting rectangular plate

2. MATHEMATICAL CONSIDERATIONS AND ANALYTICAL RESULTS

The boundary conditions (5) may be written down as follows:

$$\frac{\partial^2 \Pi_{1z}^{(s)}}{\partial z'^2} + k^2 \Pi_{1z}^{(s)} = -E_0 e^{ik\delta/2}, \quad k\delta/2 \ll 1. \tag{6}$$

Here, due to (3):

$$\Pi_{1z}^{(s)} = C \int_{a/2}^{a/2} \int_{b/2}^{b/2} J(y', z') \frac{e^{-ikr_s}}{r_s} dy' dz' \tag{7}$$

$$r_s = \sqrt{\left(\delta/2\right)^2 + (y" - y')^2 + (z" - z')^2} \tag{8}$$

The general solution of the differential equation (6) is:

$$\Pi_{1z}^{(s)} = -\frac{E_0}{k^2} + A(y")coskz" + B(y")sink|z"| \tag{9}$$

where A and B are integration constants. Equating expressions (7) and (9) we get:

$$C \int_{a/2}^{a/2} \int_{b/2}^{b/2} J(y', z') \frac{e^{-ik\sqrt{\left(\delta/2\right)^2 + (y"-y')^2 + (z"-z')^2}}}{\sqrt{\left(\delta/2\right)^2 + (y"-y')^2 + (z"-z')^2}} dy' dz' = -\frac{E_0}{k^2} + Acoskz" + Bsink|z"| \tag{10}$$

This is the fundamental, two-dimensional integral equation of our problem, where the unknown function $J(y', z')$ should be determined, being the surface density of the axial current arising at the plate [3]. Let us multiply and divide by *k* the left side of this integral equation and then overwrite it as follows:

$$\int_{a/2}^{a/2}\int_{b/2}^{b/2} J(y', z')K(y' - y", z' - z")dy'dz' = F(z", y") \tag{11}$$

$$K(y" - y', z" - z') = kC\frac{e^{-ik\sqrt{\left(\delta/2\right)^2+(y'-y")^2+(z'-z")^2}}}{\sqrt{\left(\delta/2\right)^2+(y'-y")^2+(z'-z")^2}} \tag{12}$$

$$F(z", y") = -\frac{E_0}{k^2} + A(y")coskz" + B(y")sink|z"| \tag{13}$$

Expression (12) represents the kernel of the integral equation, in $M' = M"$ point its value is $K(\theta, 0) = e^{ik\delta/2}\Big/ k\delta/2$ or $|K(\theta, 0)| = 2/k\delta \gg 1$, and, due to it, it has very high peak. In this case it belongs to the class of δ-like functions and may be presented in an approximate way:

$$K(y' - y", z' - z") = Q\delta(y' - y", z' - z") \tag{14}$$

where Q is the normalizing factor.

Inserting (14) into (11) yields:

$$QJ(y", z") = -M + A(y")coskz" + B(y")sink|z"|, \quad (M < \frac{E_0}{k^2}) \tag{15}$$

where $A(y")\ and\ B(y")$functions have to be determined. For this purpose let us apply two conditions : the value of the axial current at upper and lower ends of the plate should be zero, i.e. $J\left(y", \pm b/2\right) = 0$, and the following equation is found:

$$A(y")cos\beta + B(y")sin\beta = M, \quad \left(\beta = \frac{kb}{2} = \frac{\pi b}{\lambda}\right) \tag{16}$$

Another equation connecting $A(y")\ and\ B(y")$ coefficients may be received due to the following consideration: assume in (15) $z" = 0$, which yields:

$$QJ(y",0) = -M + A(y") \; or \; A(y") = M + QJ(y",0) \tag{17}$$

where $J(y",0)$ represents the dependence of the axial current on the transversal y-coordinate in the midline of the plate along Y-axis in $-a/2 \le y" \le a/2$ range. This dependence should be exactly the same as for diffraction of E-polarized wave at the thin metal stripe. The exact value of this current is given as follows [4]:

$$J(y",0) = \frac{K(\alpha)}{\pi Z_0}\left\{\pi[\delta(\alpha + ky") + \delta(\alpha - ky")] + \frac{1}{\sqrt{\alpha^2 - k^2 y"^2}}\right\} \tag{18}$$

$$K(\alpha) = \frac{2}{H_0^{(1)}(\alpha) - J_0\left(\frac{\alpha}{2}\right)H_0^{(1)}\left(\frac{\alpha}{2}\right)}, \quad \alpha = \frac{ka}{2}, \quad Z_0 = 120\pi\ \Omega.$$

Eq. (18) should be inserted into the right-hand-side of (17) and, thus, the value of $A(y")$ function will be determined unambiguously. Then, we easily determine $B(y")$, as well from (16).

Finally, for the axial current arising at the surface of the plate, from eq. (15) we obtain:

$$J(y",z") = -M + Mcoskz - Qcoskz"J(y",0) + sinkz" \cdot Qctan\beta J(y",0) + \\ + Msink|z"|\frac{1-cos\beta}{sin\beta} \tag{19}$$

It may be easily checked out that this expression satisfies $J\left(y', \pm b/2\right) = 0$ condition. And now let us count the value of θ coefficient, which is the normalized multiple in (14). Introducing notations by: $y' = \frac{a}{2}\xi$, $y = \frac{a}{2}\xi$, $z' = \eta\frac{b}{2}$, $z" = \eta'\frac{b}{2}$ we write eq. (14) as follows:

$$K\left(\frac{a}{2}|\xi - \xi'|, \frac{b}{2}|\eta - \eta'|\right) = Q\delta\left(\frac{a}{2}|\xi - \xi'|, \frac{b}{2}|\eta - \eta'|\right) \tag{20}$$

Furthermore, by introducing additional notations $\tau_1 = \xi - \xi'$, $\tau_2 = \eta - \eta'$ conclude then that, as to ξ, ξ', η, η' variables vary within the closed interval $(-1 \le \xi, \xi', \eta, \eta' \le 1)$, τ_1, τ_2 variables then should be placed inside $(-2 \le \tau_1, \tau_2 \le 2)$ interval and eq. (20) can be written as follows:

$$K\left(\frac{a}{2}\tau_1,\frac{b}{2}\tau_2\right)=Q\delta\left(\frac{a}{2}\tau_1,\frac{b}{2}\tau_2\right) \tag{21}$$

Integrating it by both τ_1,τ_2 variables from $-2\ to\ 2$, we obtain:

$$\int_{-2}^{2}\int_{-2}^{2}K\left(\frac{a}{2}\tau_1,\frac{b}{2}\tau_2\right)d\tau_1 d\tau_2=Q \tag{22}$$

According to eq. (12) we have:

$$\int_{-2}^{2}\int_{-2}^{2}K\left(\frac{a}{2}\tau_1,\frac{b}{2}\tau_2\right)d\tau_1 d\tau_2=\int_{-2}^{2}\int_{-2}^{2}kC\frac{e^{-ik\sqrt{\left(\delta/_2\right)^2+\frac{a^2}{4}{\tau_1}^2+\frac{b^2}{4}{\tau_2}^2}}}{\sqrt{\left(\delta/_2\right)^2+\frac{a^2}{4}{\tau_1}^2+\frac{b^2}{4}{\tau_2}^2}}d\tau_1 d\tau_2$$

Let us use, now, that $K\left(\frac{a}{2}\tau_1,\frac{b}{2}\tau_2\right)$ function is finite from the physical point of view, in particular:

$$K\left(\frac{a}{2}\tau_1,\frac{b}{2}\tau_2\right)\neq 0, when\ |\tau_1|,|\tau_2|\leq 2$$

$$K\left(\frac{a}{2}\tau_1,\frac{b}{2}\tau_2\right)\neq 0, when\ |\tau_1|>2\ or\ |\tau_2|>2$$

That is why we may infinitely increase, say τ_1 within the borders of integration, arriving then to the following expression [instead of eq. (22)]:

$$Q=i\pi kC\int_{-2}^{2}H_0^{(2)}\left(k\sqrt{\left(\delta/_2\right)^2+\frac{a^2}{4}{\tau_1}^2}\right)d\tau_1 \tag{23}$$

Here we used the relation:

$$\int_{-\infty}^{\infty}\frac{e^{-ik\sqrt{\left(\delta/_2\right)^2+\frac{a^2}{4}{\tau_1}^2+\frac{b^2}{4}{\tau_2}^2}}}{\sqrt{\left(\delta/_2\right)^2+\frac{a^2}{4}{\tau_1}^2+\frac{b^2}{4}{\tau_2}^2}}d\tau_2=i\pi\int_{-2}^{2}H_0^{(2)}\left(k\sqrt{\left(\delta/_2\right)^2+\frac{a^2}{4}{\tau_1}^2}\right)d\tau_1$$

The integral in the expression (23) may be calculated by any quadrature formula, for example, by the rectangular formula. In given case, according to it, for three points ${\tau_1}^{(1)}=-2,{\tau_1}^{(2)}=0,{\tau_1}^{(3)}=2$, we arrive to the following result:

$$Q=i\pi kC\frac{4}{3}\left[2H_0^{(2)}\left(k\sqrt{\left(\delta/_2\right)^2+4^6}\right)+H_0^{(2)}\left(k\,\delta/_2\right)\right] \tag{24}$$

As to $H_0^{(2)}\left(k\,\delta/2\right)$ is a large number, in (19) all terms including Q are dominant and, thus, instead of (19) we write approximately:

$$J(y",z") \approx -Q(sinkz"ctan\beta - coskz")J(y",0) \tag{25}$$

This expression represents the approximate solution of the integral equation (11) being the more exact, the stronger is $k\,\delta/2 \ll 1$(*) inequality.

Now let us take into account the radiation characteristic of the plate. First of all, we should write down the expression of Green's function e^{-ikr}/r in the far zone:

$$\frac{e^{-ikr}}{r} \approx \frac{e^{-ikR}}{R} \cdot e^{-iky' sin\varphi sin\theta - ikz' cos\theta}$$

Then, we insert this expression into eq. (3). From this, we obtain:

$$\Pi_{1z} = C\,\frac{e^{-ikR}}{R} \cdot \iint_{-a/2\,-b/2}^{a/2\;b/2} J(y',z') e^{+iky' sin\varphi sin\theta + ikz' cos\theta}\, dy'dz' \tag{26}$$

while from eq. (25) we obtain:

$$\Pi_{1z} = CQ\,\frac{e^{-ikR}}{R} \int_{-a/2}^{a/2}\int_{-b/2}^{b/2} (sinkz"ctan\beta - coskz")J(y",0) \times$$
$$\times\, e^{iky" sin\varphi sin\theta + ikz" cos\theta}\, dy\,dz \tag{27}$$

where $J(y",0)$ is provided by eq. (18). Values of arising integrals are provided below $\left(\beta = \pi\frac{b}{\lambda}\right)$:

$$f_1(\theta) = \int_{-b/2}^{b/2} sinkz" e^{ikz" cos\theta}\, dz" = \frac{b}{2\beta}\left[\frac{sin\beta(1-cos\theta)}{1-cos\theta} - \frac{sin\beta(1+cos\theta)}{1+cos\theta}\right] \tag{28}$$

$$f_2(\theta) = \int_{-b/2}^{b/2} coskz" e^{ikz" cos\theta}\, dz" = \frac{b}{2\beta}\left[\frac{sin\beta(1-cos\theta)}{1-cos\theta} - \frac{sin\beta(1+cos\theta)}{1+cos\theta}\right] \tag{29}$$

$$f_3(\theta,\varphi) = \int_{-a/2}^{a/2} J(y'',z'') e^{iky'' sin\varphi sin\theta}\, dy" =$$

$$= \frac{K(\alpha)}{\pi Z_0}\int_{-a/2}^{a/2} e^{iky'' sin\varphi sin\theta}\left\{\pi[\delta(\alpha + ky") + \delta(\alpha - ky")] + \frac{1}{\sqrt{\alpha^2 - k^2 y"}}\right\} dy" =$$

$$= \frac{K(\alpha)}{kZ_0}[2cos(\alpha sin\varphi sin\theta) + J_0(\alpha sin\varphi sin\theta)], \quad \left(\alpha = \frac{ka}{2}\right) \tag{30}$$

Furthermore, it is appropriate to write down eq. (27) in the following compact form:

$$\Pi_{1z} = CQ\frac{e^{-ikR}}{R}[f_1(\theta)ctan\beta - f_2(\theta) - f_3(\theta,\varphi)]$$

Using formula (2), it is possible to calculate the electric field strength in the far zone. Taking into account that $\Pi_{1z} \sim {}^{1}/_{R}$, while ${}^{\partial^2\Pi_{1z}}/_{\partial z^2} \sim {}^{1}/_{R^2}$, we cancel the second term in the right-hand side of eq. (2), then reducing it to the following expression:

$$E_{1z} = k^2\Pi_{1z}$$

Furthermore, particular interest arises to the value of the azimuthal component of the electric strength, $E_{1\theta}$, given by the following expression:

$$E_{1\theta} = E_{1z}sin\theta = k^2CQ\frac{e^{-ikR}}{R}F(\theta,\varphi)$$

where:
$$F(\theta,\varphi) = [f_1(\theta)ctan\beta - f_2(\theta) - f_3(\theta,\varphi)]sin\theta \qquad (31)$$

is the radiation pattern of the plate.

For numerical calculations it is appropriate to normalize expression (31) in $\theta = 60^0$ and $\varphi = 0$ directions. Then:

$$F(60^0,0) = \left[\frac{b}{\beta}\left(sin\frac{\beta}{2} - \frac{1}{3}sin\frac{3}{2}\beta\right)ctan\beta - \frac{b}{\beta}\left(sin\frac{\beta}{2} + \frac{1}{3}sin\frac{3}{2}\beta\right) - T\right]\frac{\sqrt{3}}{2} \qquad (32)$$

$$T = \frac{3K(\alpha)}{kZ_0}$$

For the normalized characteristic we obtain:

$$F_{nor}(\theta,\varphi,\beta) = \frac{F(\theta,\varphi,\beta)}{F(60^0,0)} =$$

$$= \frac{\frac{b}{2\beta}\left\{\left[\frac{sin\beta(1-cos\theta)}{1-cos\theta} - \frac{sin\beta(1+cos\theta)}{1+cos\theta}\right]ctan\beta - f_2(\theta) - f_3(\theta,\varphi)\right\}sin\theta}{\frac{b}{2\beta}\left[\left(2sin\frac{\beta}{2} - \frac{2}{3}sin\frac{3\beta}{2}\right)ctan\beta - f_2(60^0) - f_3(60^0,0)\right]\frac{\sqrt{3}}{2}} \qquad (33)$$

At the main meridian plane ($\varphi = 0$) the radiation pattern is represented as follows:

$$F_{nor}(\theta, 0, \beta) = \frac{\frac{b}{2\beta}[G(\theta)ctan\beta - f_2(\theta + g(\alpha))]sin\theta}{\frac{b}{2\beta}[T(\beta)ctan\beta - f_2(60^0) - f_3(60^0, 0)]\frac{\sqrt{3}}{2}} \quad (34)$$

where:

$$G(\theta) = \frac{sin\beta(1-cos\theta)}{1-cos\theta} - \frac{sin\beta(1+cos\theta)}{1+cos\theta}, \quad g(\alpha) = \frac{3K(\alpha)}{kZ_0} = f_3(\theta, \varphi) \quad (35)$$

$$T(\beta) = 2sin\frac{\beta}{2} - \frac{2}{3}sin\frac{3\beta}{2} \quad (36)$$

Consider now the special case, when $\beta = (2n+1)\pi$ or $b = (2n+1)\lambda$, where $(n = 0,1,2, \dots)$, i.e. the height of the plate is the odd number of the wavelength. In such a case, $ctan\beta = \infty$ and eq. (34) sufficiently simplifies, being transformed into the following expression:

$$F_{nor}(\theta) = (-1)^n 2\frac{sin[(2n+1)\pi cos\theta]}{sin\theta}, \quad \frac{b}{\lambda} = 2n + 1.$$

When n = 0, we obtain: $F_{nor}(\theta) = 2\frac{sin(\pi cos\theta)}{sin\theta}, \quad \frac{b}{\lambda} = 1$

while, when n = 1: $F_{nor}(\theta) = 2\frac{sin(3\pi cos\theta)}{sin\theta}, \quad \frac{b}{\lambda} = 3.$

REFERENCES

[1] L.A. Vainstein. Electromagnetic Waves. PH – ACT, Moscow, 440 p., 1988 (in Russian).

[2] F.G. Bogdanov, G.Sh. Kevanishvili. Diffraction of EM Waves on Periodic Gratings & Waveguide Discontinuities. Tbilisi, PH "Samshoblo", 1994, 244p (in Russian).

[3] G.Sh. Kevanishvili, K.V. Kotetishvili, G.G. Chikhladze et al. On the Electromagnetic Compatibility of Dipole Antenna.Georgian Engineering News(GEN), № 2, 2009.

[4] G.G. Chikhladze, G.Sh. Kevanishvili, I.G. Kevanishvili, G.G. Mushkudiani. Scattering of EM Waves on Double-Period Grating Formed of Passive Dipoles. Georgian Engineering News (GEN), № 3, 2014.

MOBILE PHONE EM EXPOSURE STUDY ON INHOMOGENEOUS HUMAN MODELS CONSIDERING DIFFERENT HAND POSITIONS

V. Jeladze, T. Nozadze, R. Zaridze, M. Prishvin, V. Tabatadze, M. Tsverava

Tbilisi State University, Laboratory of Applied Electrodynamics and Radio Engineering

3, Chavchavadze Ave. Tbilisi, Georgia

Email : tamar.nozadze002@ens.tsu.edu.ge, revaz_zaridze@mail.ru, veriko.jeladze001@ens.tsu.edu.ge

Abstract

The goal and the novelty of the proposed research is to study Mobile phone EM exposure influence upon the inhomogeneous child and woman models in case of different hand and finger positions at the 900 MHz, 1900 MHz and 3700 MHz frequencies. Numerical simulations are carried out using FDTD method to estimate the specific absorption rate (SAR) and temperature rise caused by absorption of EM field energy in the human tissues. There were also studied SAR and temperature rise dependence on S11 radiation parameter of mobile phone antenna for different distances.

1. INTRODUCTION

A tremendous increase of mobile phones and other wireless communication systems are observed during past years. Their EM radiation can be dangerous for human health. In this way the study of their EM exposure influence on the human body is very actual problem nowadays. The antenna of a mobile phone is located in a close proximity to the user's head and hand. Both are a dielectric object with high loss dielectric parameters. The wavelength is comparable to the both, head and hand and they affect the radiation process. It is important detailed study these phenomena in order to obtain some general conclusions about the nature of exposure process and to elaborate some safety recommendations and standards. It is necessary find out the way how to reduce the radiation influence on human from phone antennas.

Many researches show that radiation nature and EM fields behavior is highly dependent on complex human body geometry and anatomy [1], location in an enclosed or semi-enclosed room and its wall's transparency [2,3], other objects around the user, etc.

The researches also show that absorption of radiated energy (SAR) depends on characteristics of mobile phones, antenna types and its positions or the phantom itself, and radiated power from the mobile phone [4-7]. It is important to note that the absorption may be in the device and in the human, holding the device, but here the variations in the user influence are difficult to include. This problem is avoided if the antenna is measured in the anechoic chamber including different users as it was done in [8,9].

In [10] it two types of realistic mobile phones were considered. There have been some reports about possible effect of the hand presence on the head SAR if hand phantom is included in the measurements of the head SAR compliance assessment procedure. There was shown that lower band GSM frequencies the presence of the hand decreases the SAR in head tissues up to ~70%. For the upper band GSM frequencies, the presence of the hand decreases the head SAR up to ~55%.

In spite of many publications on this topic the problem is not studied completely. Our paper focuses on detail investigation how the hand and fingers position influence on the EM field energy absorption and temperature increase in the human (woman and child) head tissues; their dependence on S11 radiation parameter of mobile phone patch antenna; also, the fields behavior in the near and far zone.

2. MODELS, METHODS AND RESULTS OF NUMERICAL SIMULATIONS

As it mentioned above, our goal is to investigate EM field exposure on human, particularly, on a woman's and child's models, with and without considering the different hand (finger) positions and estimate SAR and temperature rise values in the head tissues. The inhomogeneous 3D models of a woman named as "Ella" and child named as "Thelonious" [11] were used with 1mm discretization.

Figure 1. Woman (Ella) head model with phone, a) without hand, b) with hand position 1, c) with hand position 2.

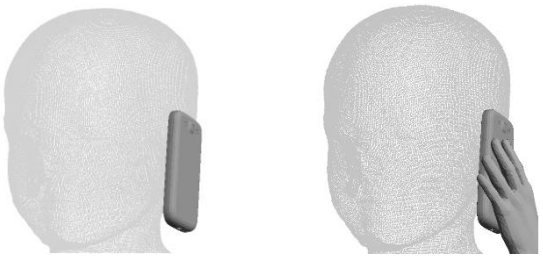

Figure 2. Child (Thelonious) 3D models with phone: a) without hand, b) with hand.

For the woman head model two hand position (Figure 1), holding the mobile phone, were selected: phone held with fingers (hand position 1) and phone held with the palm (hand position 2). For the child model, it was selected only one hand position (Figure 2b). The handset is placed from the head model at the distances 1 mm and 10 mm. For the both human model frequency dependent tissue parameters for the EM simulation and thermal tissue parameters have been used from the known database [12]. The hand models are filled with muscle material. The patch antenna is embedded in mobile phone model (Figure 2), which dimensions are 9x5x0.8 [cm]. The phone case dielectric permeability $\varepsilon=2$ and patch antenna dielectric is Bakelite, with permeability $\varepsilon=4.8$. The woman's and child's head-hand and mobile phone discrete models in different plane are presented on the figure 3 and figure 4.

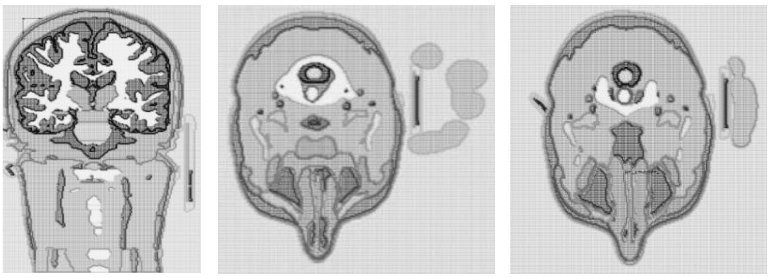

a) b) c)

Figure 3. Woman (Ella) discretic model: a) without hand, b) with hand position 1, c) with hand position 2.

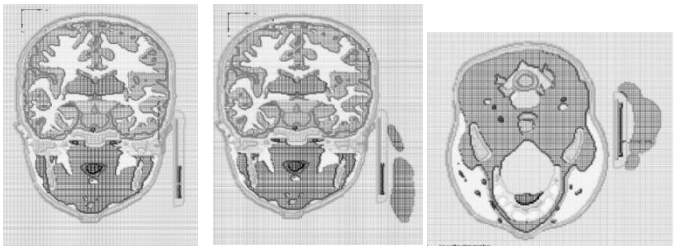

a) b)

Figure 4. Child (Thelonious) discretic head model with phone: a) without hand, b) with hand in different plane.

The numerical experiments were conducted using the EM and thermal solver, program package FDTDLab, which is developed at TSU [11, 12] and based on the FDTD method. The standard frequencies: 900, 1900, 3700 [MHz] are selected for the simulations and a sinusoidal wave signal has been used at corresponding frequency. SAR and Temperature rise in tissue were simulated due to RF exposure from mobile phone's Patch antenna placed at 1mm and 10mm distance from the head model.

3. RESULTS AND DISCUSSIONS

Based on the above-mentioned models and parameters, we have obtained the following results. The E field distributions for the Ella and Thelonious head-hand models head-hand models are shown on figures 5, 6. It can be seen from Figures 5a, 6a, that the significant part of energy is radiated into the open space; the rest is absorbed by the head. But when we take into account hand, the most part of radiated energy is absorbed by the hand; as a result, the field values inside the head will be smaller (Figures 5b, 5c, 6b).

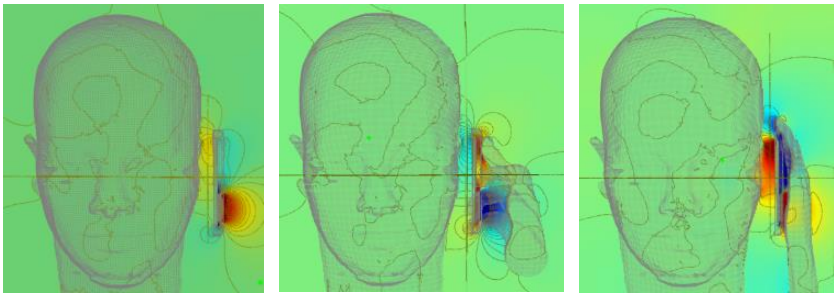

a) b) c)

Figure 5. Near field distribution for the woman (Ella) head model at 900 MHz, a) without hand, b) with hand position 1, c) with hand position 2.

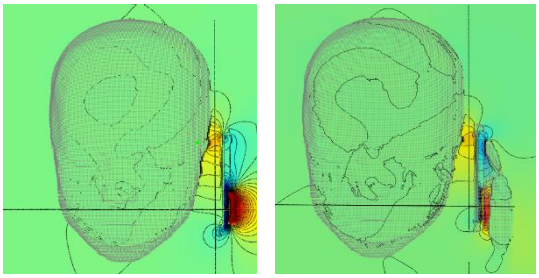

a) b)

Figure 6. Near field distribution for the child (Thelonious) head model at 900 MHz: a) without hand, b) with hand.

On figures 7, 8 are presented 3-dimentional far field patterns for the both human head without hand and with different hand positions at 900 MHz.

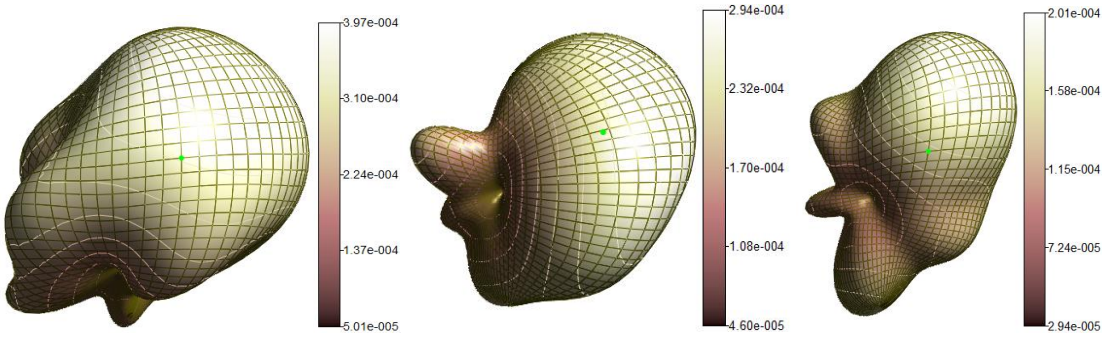

Figure 7. Far field patterns at 900 MHz for the woman (Ella) head: a) without hand, b) with hand position 1, c) with hand position 2.

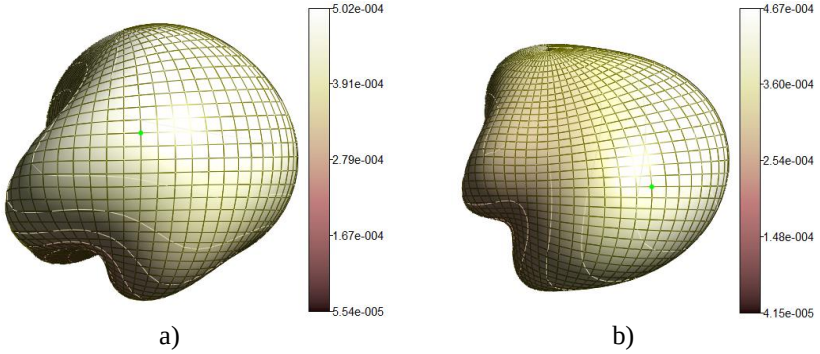

Figure 8. Far field patterns at 900 MHz for the child head: a) without hand, b) with hand.

The simulated 2-dimentional radiation patterns for different scenarios with some positions of the antenna, the head and the hand are presented on figures 9, 10. From figures it's clearly seen, that hand presence changes the radiation pattern and its quantity. The head and hand palm (hand position 2) absorbs the most part of the energy radiated by the phone, that's why the far field pattern size is much smaller than in the case when the phone is held by the fingers (hand position 1) and than in other cases (Figure 9). We have a similar picture for the child model (Figure 10).

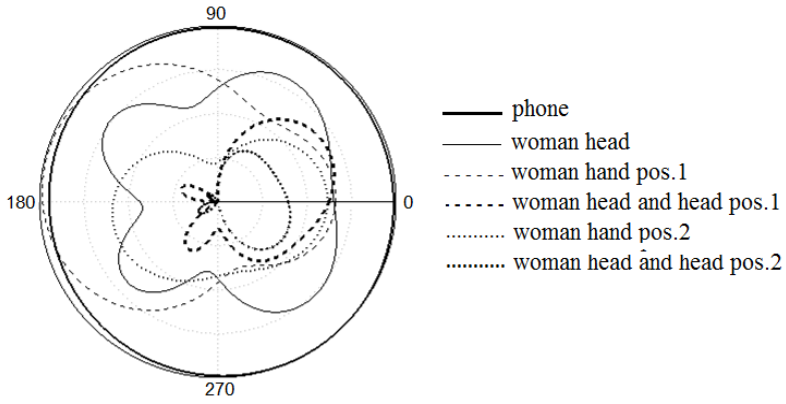

Figure.9. Radiation pattern of the woman model "head-hand" system at 900 MHz radiation Frequency.

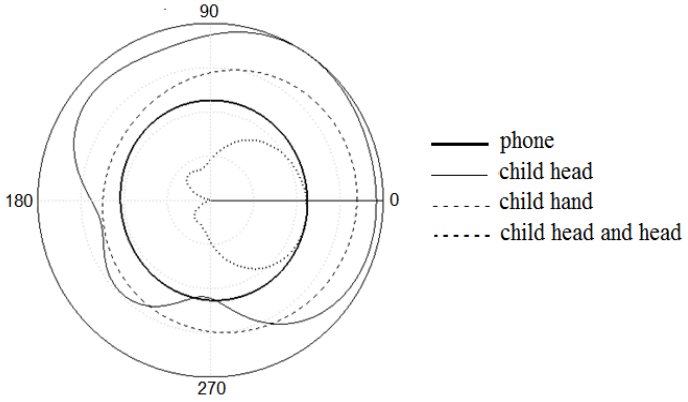

Figure 10. Radiation pattern of the child model "head-hand "system at 900 MHz radiation Frequency.

On figures 11 and 12, SAR distributions for the Ella and Thelonious head-hand models are shown at 900 MHz radiation frequency.

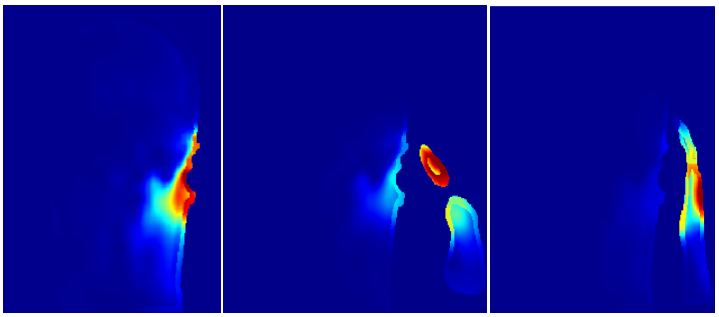

a) b) c)

Figure 11. SAR distribution for the woman (Ella) head and hand models at 900 MHz, a) head without hand, b) head with hand position 1, c) head with hand position 2.

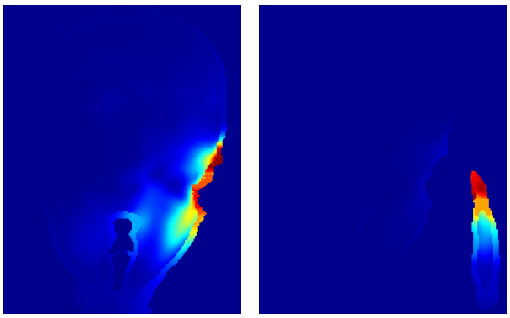

a) b)

Figure 12. SAR distribution for the child (Thelonious) head and hand models at 900 MHz, a) head without hand, b) head with hand.

It can be seen that when hand is considered the peak SAR locations are shifted from the head to the hand, because hand absorbs a big part of radiated energy and as a result, the peak values of SAR in the head model are drastically reduced.

This good effect seems from the figures 13, 14 where the 10g SAR peak values for the woman and child head models without hand and considering hand different positions are given, when hand and phone are placed at 1 mm and 10 mm distances from the head model. All the obtained results are normalized for the 1W of input power.

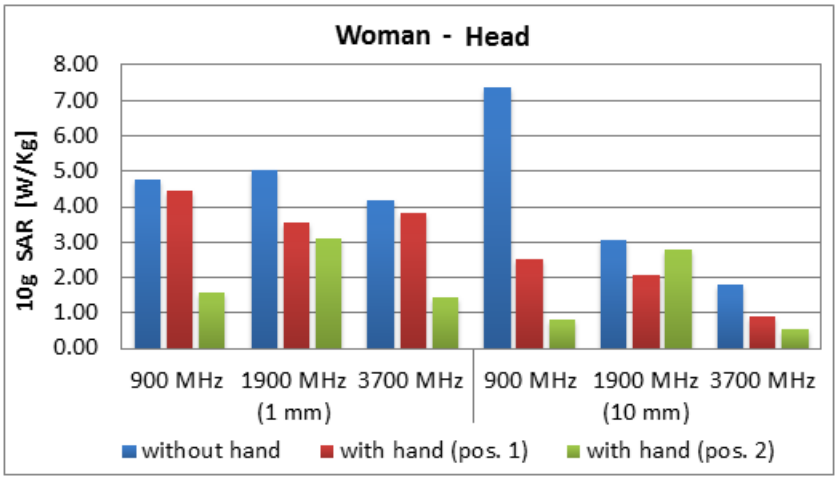

Figure 13. 10g SAR values for the woman (Ella) head model at 900 MHz, 1900 MHz and 3700 MHz, without hand and considering the hand position 1, hand position 2.

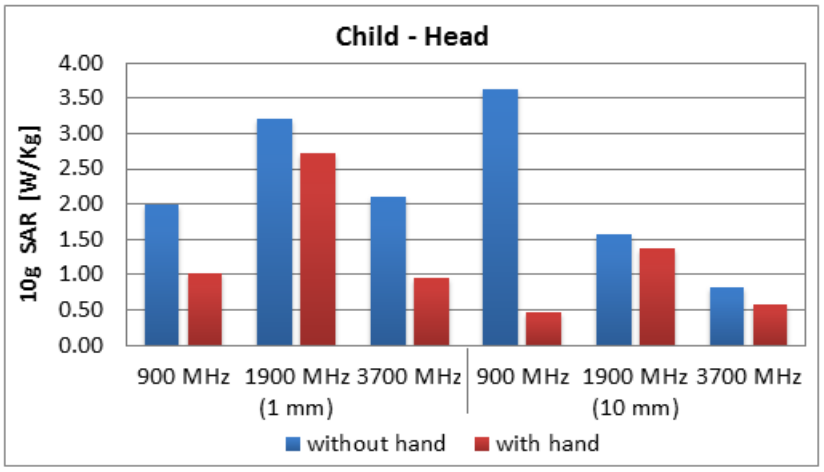

Figure 14. 10g SAR for the child (Thelonious) head model at 900 MHz, 1900 MHz and 3700 MHz, with and without hand.

According to the results, which are presented in figure 13, 10g SAR peak values in the head considering the hand position 2 are much smaller than for hand position 1.

The temperature rise peak values in the woman and child head models, for the considered head-hand models, when the distances between them are 1 mm and 10 mm, are presented on figures 15, 16.

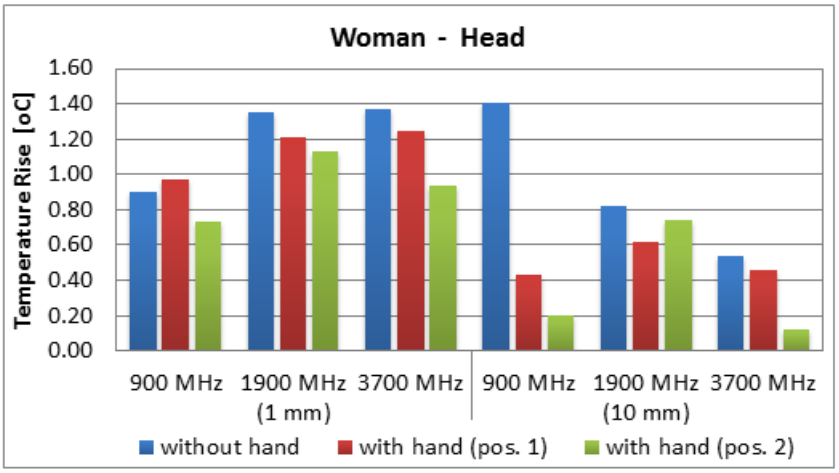

Figure 15. Temperature rise for the Ella head model at 900 MHz, 1900 MHz and 3700 MHz, without hand and for the hand position 1, hand position 2.

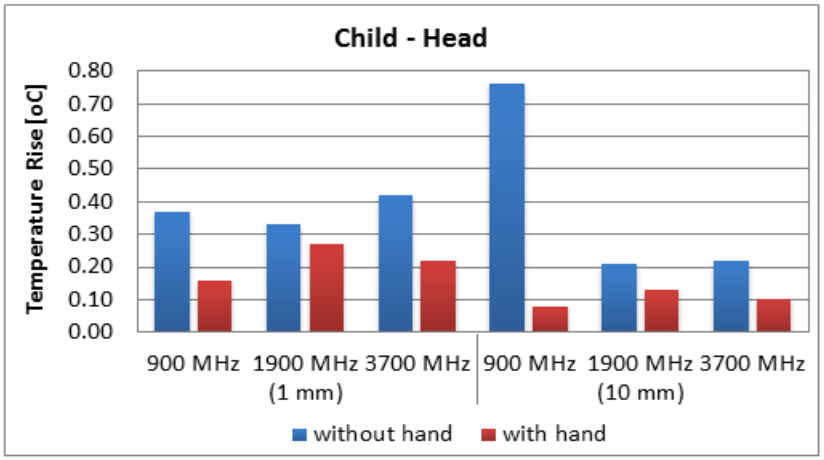

Fig.16 Temperature rise for the child (Thelonious) head model at 900 MHz, 1900 MHz and 3700 MHz, with and without hand.

All presented results show that if we take into account the hand effect, we see the reduction of SAR and temperature rise values in a woman and child head tissues. It has been also shown that if phone is held by a palm (hand position 2) SAR and temperature rise are lower than in case when phone held with fingers (hand position 1). This is explained the fact that the most part of radiation is absorbed in the palm and just a small part of radiation reaches the woman head. The SAR and temperature rise values also depend on distance between the head model and the phone with hand models. In particular, these values are higher when the radiation source with hand is close to the head (for 1 mm) than for the 10 mm 20 mm distance from it, because EM field is inversely proportional to the distance from the source. After that we have investigated SAR and temperature rise dependences on mobile phone's antenna radiation S11 parameter. The obtained results are presented on Figures 17, 18.

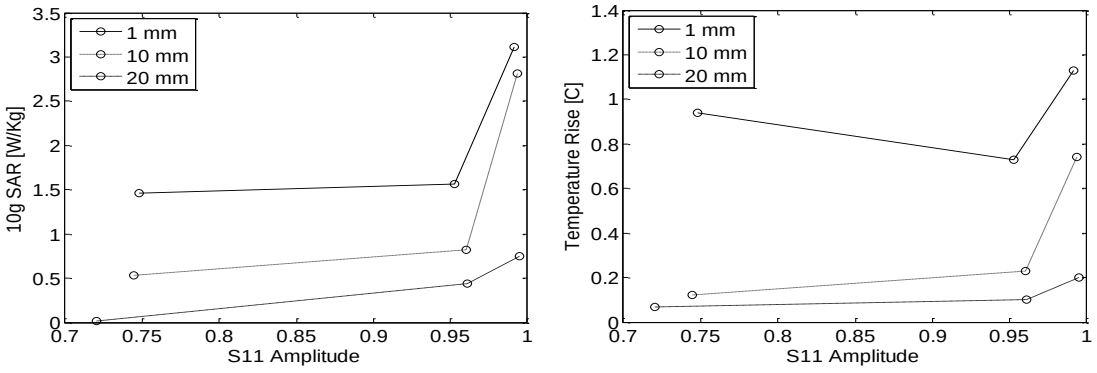

Figure 17. (a) 10g SAR and (b) Temperature Rise dependences on S11 for woman head model considering hand pos. 2. SAR normalized to 1W input power.

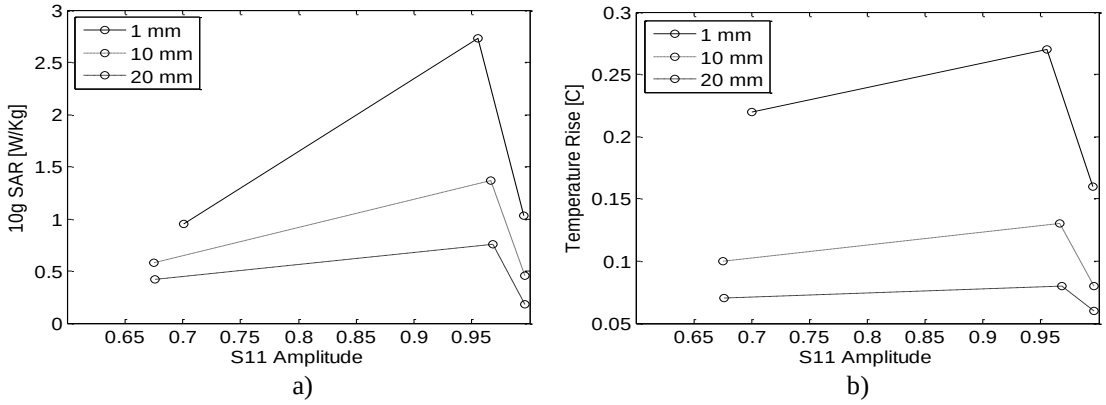

Figure 18. (a) 10g SAR and (b) Temperature rise dependences on S11 for child head model. Temperature rise normalized to 1W.

As it can be seen from figures 18a, 18b for the examined scenarios SAR and temperature rise values increase with the increase of S11 coefficient. Though it is a proofed fact, that there is a strict correlation between S11 and temperature rise. On the figures 19a, 19b we see that some points are not in agreement with previously observed dependency.

The relative position of the head, hand and handset determines the radiation condition, for some of examined scenarios the S11 close to 1.0 means, that almost nothing is radiated. Despite the fact, that the obtained results are normalized for the 1W of input power, these results where the S11 was close to 1.0 are not reliable and can be neglected. From the above stated we can conclude that the amount of energy absorbed by human tissues can be estimated by monitoring the S11 coefficient.

4. CONCLUSIONS

The effects, related to the presence of a human hand, holding the mobile phone, and the EM exposure process have been studied in this paper. It has been shown that the hand presence changes the radiation pattern, thus changing the SAR and temperature rise peak values in tissues. The peak SAR and temperature rise values in the head tissues are lower considering the hand presence. These values are even more reduced in the head tissues when phone held with a palm than in case when the mobile phone held with fingers, because most part of radiation is absorbed by palm. Also, resultant SAR and temperature rise values are decreasing by increasing the distance from the radiation

source to the head. Based on the obtained results we can make the following safety recommendation. If phone hold with palm the most part of the radiated energy is absorbed in it. In this occasion, it is better not to cover the mobile antenna by the palm, because modern smartphones automatically increase the radiated power to achieve good connection, causing higher SAR and temperature rise values in the head tissues. It is better to hold the phone with finger tips as far from the head as possible in order to reduce EM field exposure. It is shown that in first approximation the peak SAR and temperature rise value depend on the S11 coefficient. And the amount of energy absorbed by human tissues can be estimated by monitoring the S11 coefficient, making the smartphones even smarter. Finally, it should be noted that every human is unique and differs in form, dimensions, weight and constitution, thus it's difficult to make general conclusions. Due to this reason, the stated problems still are topical nowadays and it requires further research.

ACKNOWLEDGEMENT

This work is supported by the Shota Rustaveli National Science Foundation grant [Grant No: YS15_2.12_56].

REFERENCES

[1] V. Jeladze, M. Prishvin, R. Zaridze, "RF Exposure Simulation using Considering Blood Perfusion for a Child and Woman Models", Journal of Applied Electromagnetism (JAE), Vol. 16, No.2, 2014, pp. 26-33.

[2] V. Jeladze, V. Tabatadze, M. Prishvin, I. Petoev, R. Zaridze, "Influence of the Walls Transparency on the Resonant EM Field's Values," Journal of Applied Electromagnetism (JAE), vol. 18, no. 1, pp. 1-13, June 2016.

[3] V. Jeladze, I. Petoev, V. Tabatadze, M. Prishvin, R. Zaridze, "Application of the Method of Auxiliary Sources to Study the Influence of Resonance Electromagnetic Fields on a Man in Large Spatial Domains", Journal of Communiations Technology and Electronics, Vol. 62, No.3, March 2017, pp. 195-204.

[4] J. Wiart, C. Dale, A.V. Bosisio, A. Le Cornec, "Analysis of the influence of the power control and discontinuous transmission on RF exposure with GSM mobile

phone," IEEE Transactions on Electromagnetic Compatibility, vol. 42, no. 4, pp. 376-385, 2000.

[5] M. R. I. Faruque, M. T. Islam, N. Misran, "Design of metamaterial attachment for SAR reduction in human head," Applied Computational Electromagnetic Society Journal, vol. 25, no. 12, pp. 1097-1107, 2010.

[6] B.B. Beard, W. Kainz, T. Onishi, et al. "Comparisons of Computed Mobile Phone Induced SAR in the SAM Phantom to that in Anatomically Correct Models of the Human Head," IEEE Transactions on Electromagnetic Compatibility, vol. 48, no. 2, pp. 397- 407, 2006.

[7] M. R. I. Faruque, M. T. Islam, N. Misran, "Effects of dielectric values & substrate materials on electromagnetic (EM) absorption in human head," Frequenz–Journal of RF-Engineering and Telecommunications, vol. 66, no. 3-4, pp. 79-83, 2012

[8] G. F. Pedersen, M. Tartiere, and M. B. Knudsen, "Radiation efficiency of handheld phones," in *Proc. 50th Veh. Technol. Conf.*, May 2000, pp. 1381–1385.

[9] J. Krogerus, J. Toivanen, C. Icheln, and P. Vainikainen, "Effect of the human body on total radiated power and the 3-d radiation pattern of mobile handsets," *IEEE Trans. Instrum. Meas.*, vol. 56, no. 6, pp. 2375–2385, Dec. 2007.

[10] J. Keshvari1, M. Kivento," Hand Effect on Head Specific Absorption Rate (SAR) Exposed by Two Realistic Phone Models", IOP science, Materials Science and Engineering 44 (2013) 012017.

[11] IT'IS Foundation. http://www.itis.ethz.ch/virtual-population/virtual-population-cvip-vip/cvip3-and-vip1/ella/

[12] IT'IS Foundation. http://www.itis.ethz.ch/virtual-population/tissue-properties/database /database/database-summary/

[13] M. Prishvin, L. Bibilashvili, R. Zaridze, "Developing a thermal exemptions rationale for low-power transmitters". Journal of Applied Electromagnetism, vol. 13, no. 1, June 2011, pp. 39-57.

[14] M. Prishvin, L. Bibilashvili, V. Tabatadze, R. Zaridze, "Supplementary analysis of RF exposure simulations of low-power transmitters". Journal of Applied Electromagnetism, Vol.13, no 1, June 2011, pp. 58-69.

THE EFFECT OF WEATHER ON QUALITY OF EXPERIENCE IN OPTICAL WIRELESS COMMUNICATION SYSTEM (selected from CEMA'17 Conference)

Rasa Bruzgiene[*], Lina Narbutaite[*], Erich Leitgeb[**], Pirmin Pezzei[**], Thomas Plank[**]

[*] Kaunas University of Technology,

K. Donelaičio g. 73, 44249, Kaunas, Lithunia.

[**] Graz University of Technology

Rechbauerstraße 12, 8010 Graz, Austria

Email: rasa.bruzgiene@ktu.lt

Abstract

Optical Wireless communication systems are a good competitor to other wireless communication technologies in relation of its capacity to deliver high-speed broadband traffic. The way optical wireless transceivers operate is more or less the same as fiber optics ones; however, since laser signals are transferred through the atmosphere, the path loss between the transmitter and the receiver is getting raised due to various external factors (conditions) that appear on weather. The characteristics of optical wireless systems and its changes in the face of different weather conditions strongly affect the parameters of Quality of Service. Also, this influence provides the possibility to quantify the significance of the service disruption impact to the metrics of Quality of Experience. Due to this, this paper gives a new approach to the relation of the characteristics of optical wireless communication system, known as Free Space Optics, affected during the weather-based disruptions with the parameters of Quality of Service. Furthermore, this relation is used in estimation of Quality of Experience metrics.

1. INTRODUCTION

Optical Wireless (OW) systems are the good example of the integration between optical and wireless radio communications, where the light of different types is caring the main signal for data transmission over the atmospheric channel. The basic Optical Wireless system consists of three main parts (Fig. 1) - source system (optical transmitter, a modulator and an irradiation device – a telescope or a lens), channel for signal transmission and receiver system (a detector, a decoder, and a telescope or a lens).

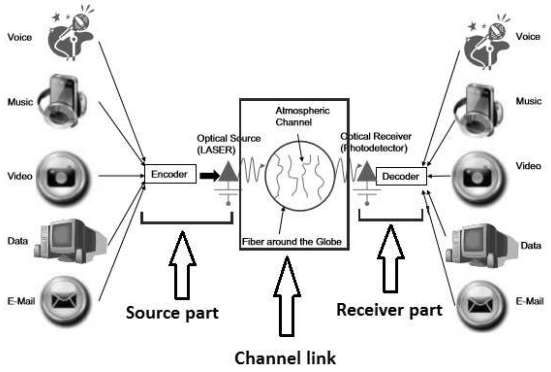

Figure 1. Structure of Optical Wireless communication system [modified from [1]].

In OW system, the information from the optical transmitter is modulated on a collimated beam of light, which is projected through free air channel onto the receiver side [1]. The channel for signal transmission is a free space (air). Since the medium for signal carrier is a light, such system operating frequencies are very high and range from 300 GHz to 300 PHz. It includes infrared (750 nm – 1mm), visible (390-750 nm) and ultraviolet bands (200-280 nm) [2]. Due to this, Optical Wireless communication can be classified into Free Space Optics (FSO), Visible Light Communication (VLC) and Ultraviolet Communication (UVC). FSO, known as terrestrial point-to-point OW communication system, offers a cost-effective protocol-transparent link with high data rates (as 10 Gbps per wavelength). Such system allows to set up communication links between two locations whenever a free line of sight is pre- sent [2]. Typical wavelength of Free Space Optics system ranges from 800 to 1700 nm. For this rea- son, Optical Wireless communication system can be used in cellular backhauls, wireless MAN extensions, WLAN-to-WLAN connectivity in different environments, broadband access to remote or underserved areas [2] etc. Also, Optical Wireless system can be used not only for temporal installations, but as well in the face of a crisis for emergency and medical needs or permanent connections in last mile access without cabling.

However, a key disadvantage of Optical Wireless systems is its sensitivity to atmospheric conditions and its limited reliability. The resilience of such systems against fast-time-changing disruptions is dependent to different weather conditions as fog, snow, rain, clouds and etc. In general, for a higher resilience of such systems it is important to identify the appropri- ate acceptable level of service over weather-based disruptions.

Acceptable level of service can be re- fined based on the service disruption impact to a user. And the Quality of Service and Quality of Ex- perience plays a key role in this way.

The paper is organized as follows: Section 2 describes investigations in order to analyze the impact of different weather conditions to the links of Optical Wireless System. Section 3 gives the solution for the correlation of optical wireless signal attenuation during the different weather conditions (with main focus to fog and clouds) to the bit error rate para- meter during the service transmission over Optical Wireless system. The results from the correlation will be used as a main input for evaluation of the objective Quality of Experience metrics in Section 4. Finally, section 5 presents the conclusions and recommendations for further investigations.

2. IMPACT OF DIFFERENT WEATHER CONDITIONS TO OW LINKS

The atmosphere is composed of gas molecules, water vapor, aerosols, dust and pollutants, whose sizes are comparable to the wavelength of a typical optical carrier affecting the carrier wave propagation not common to a radio frequency (RF) system [2]. Absorption and scattering due to particulate matter may significantly attenuate the transmitted optical signal, while the wave-front quality of a signalcarrying laser beam transmitting through the atmosphere can be severely degraded, causing intensity fading, increased bit error rates, and random signal losses at the receiver. Due to this, the atmospheric channel for signal propagation over FSO communication has to deal with many external factors related to the different weather conditions [3]: rain, fog, sleet, snow, smog, clouds, different kinds of aerosols, variations in temperature and etc. All these weather conditions affect the wireless systems and Optical Wireless systems as well. It is just a difference in a scale of the affect to the parameters of OW communication performance.

The research group of the Institute of Microwave and Photonic Engineering in TU-Graz (Austria) has done a lot of work by investigating the impact of different weather conditions to the Optical Wireless communication, especially Free Space Optics sys- tems. One test of their many investigations was do- ne with a Multi-beam system [4]. This system was installed to connect the Department of Communications and Wave

Propagation to the "Observatory Lustbühel" [5]. Fig. 2 shows a terrain profile of this system [5]. The distance between FSO units was 2.7 km.

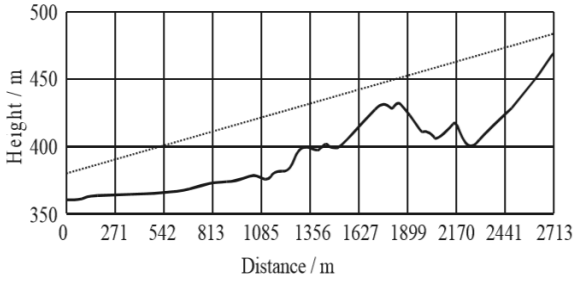

Figure 2. Terrain profile of FSO system [5].

Test data at 155 Mbps was sent from one FSO-unit to a distant FSO-unit. The received data was sent back (loop) to the first unit. As a reference to the link quality, weather data was recorded (including temperature, humidity, wind speed and direction and rain rate). The authors in this work [4] stated, that the main cause for failure of FSO links was fog. The same reason for OW system vulnerability was found in other investigation [6], comparing the fog attenuation for 850 and 950 nm wavelength in FSO system (Fig. 3).

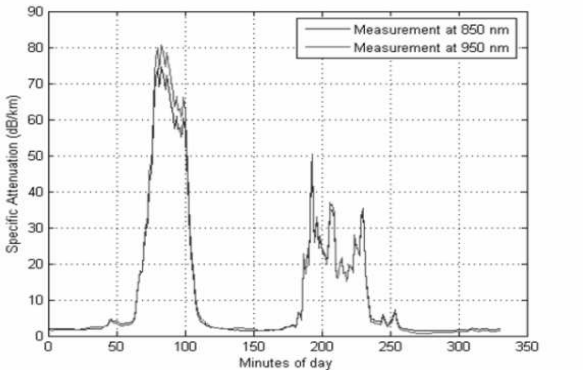

Figure 3. Influence of fog [6].

In general, fog and water clouds mostly affect FSO links due to the size of it droplets. The size of droplets is of the same order of magnitude as wave- length, which implies a high extinction efficiency, and their concentration is much larger than the one of rain or snow.

Rain is also an important attenuator for the optical signals. Fig. 4 shows that in period of a drizzle the mean power was decent by 2.5 dB at a rain rate of 2 mm/h.

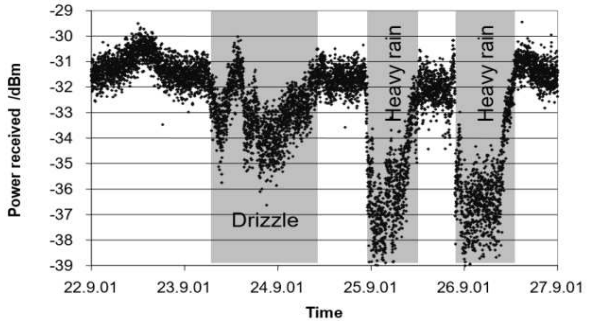

Figure 4. Influence of rain [7].

At the start of heavy rain with an average rain rate of 5 mm/h, accordingly the received power decent by 6 dB [7].

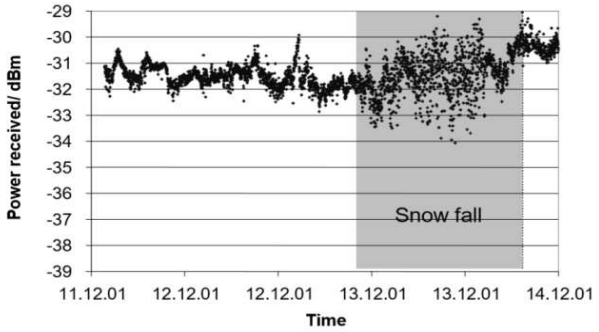

Figure 5. Snow influence [7].

Snow is usually constituted by aggregates of ice crystals and snowflakes have irregular shape or different compositions. A laser attenuation by falling snow can exceed 40 dB/km, depending on water content of snowflakes and on precipitation rate. In the investigation [7], which results are presented in Fig. 5, the received mean power of OW link stays unchanged, but the variance is increased significantly.

3. CORRELATION BETWEEN OPTICAL WIRELESS SIGNAL ATTENUATION AND QOS/QOE

As we can see in the previous section, performances characteristics of a data system over FSO links depend upon the atmosphere in which it propagates. Each wireless channel has a computable Bit Error Rate (BER), which is the probability of the occurrence of an error during data transfer over that link. As fog mostly affects the quality of FSO links comparing to other weather conditions such as rain or snow, further investigations were focused just on its effect.

Visibility is one of the parameters, which describes fog. The specific attenuation for both Kim and Kruse model is given by common empirical model [8]:

$$a(\lambda) = \frac{3.19}{V} \cdot \left(\frac{\lambda}{550}\right)^{-\gamma} \quad (1)$$

where λ is operating wavelength (nm), V is stands for visibility range(km) and g indicates the atmospheric attenuation coefficient according to Kim or Kruse model.

The BER calculation is given by the following formula:

$$BER = \frac{1}{2} erfc\left(\frac{1}{2}\sqrt{SNR}\right) \quad (2)$$

Quality assessment was carried out using SNR BER and MOS indicators, calculated by using hard- ware and software tools. Empirical values of BER transitions from an acceptable quality to the poor, according to the relationship between SNR and MOS, are presented in Table 1 [9].

For the evaluation of BER influence to QoS/QoE, we simulated two different types of fog (thick (0.2 m of visibility) and moderate (0.8 m of visibility) for two wavelengths: 1550 nm and 830 nm.

Table 1. Relationship between SNR BER and MOS [9]

MOS(%)	BER	SNR
100-81	$<10^{-8}$	>37
80-61	$10^{-8} < x < 10^{-6}$	31-37
60-41	$10^{-6} < x < 10^{-4}$	25-31
40-21	$10^{-4} < x < 10^{-2}$	20-25
<20	$>10^{-2}$	<20

We chose these parameters, because the main idea was to evaluate QoE for several types of in- formation: image and data.

4. EVALUATION OF OBJECTIVE QOS METRICS

The simulation was done using Matlab2017a software. At first, we calculated the received power and BER. The results are presented in Figs. 6 and 7.

It can be seen, that the impact of the fog to OW link depends on the length of waves over FSO system. The shorter wavelength in OW link gives a possibility to

transmit service of a good quality at least ~100 meters further during a thick or moderate fog. The lines on the different BER values presents a level of perceived QoE by the user.

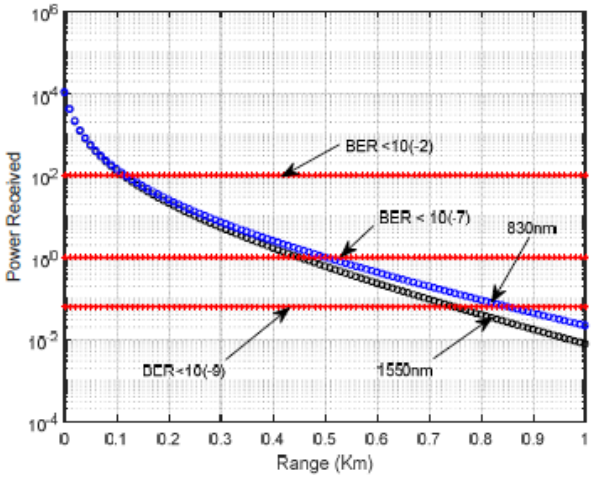

Figure 6. Thick fog.

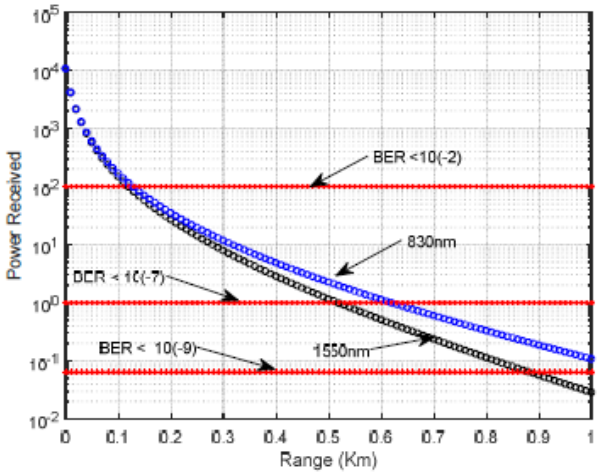

Figure 7. Moderate fog.

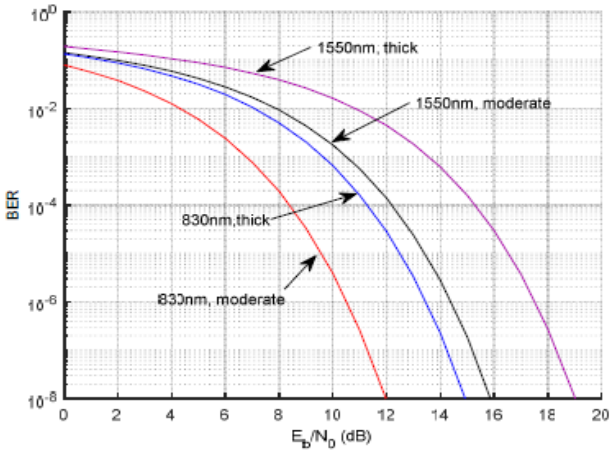

Figure 8. Relationship between BER and SNR.

The results in Fig. 8 showed, what range we need to have SNR (or Eb/N0) for different BER values.

For evaluation of MOS and QoE was used image and data information. The simulation was done for QAM-126 modulation, and SNR was between 4 and 27 dBm. The image simulation results are presented in the Fig. 9.

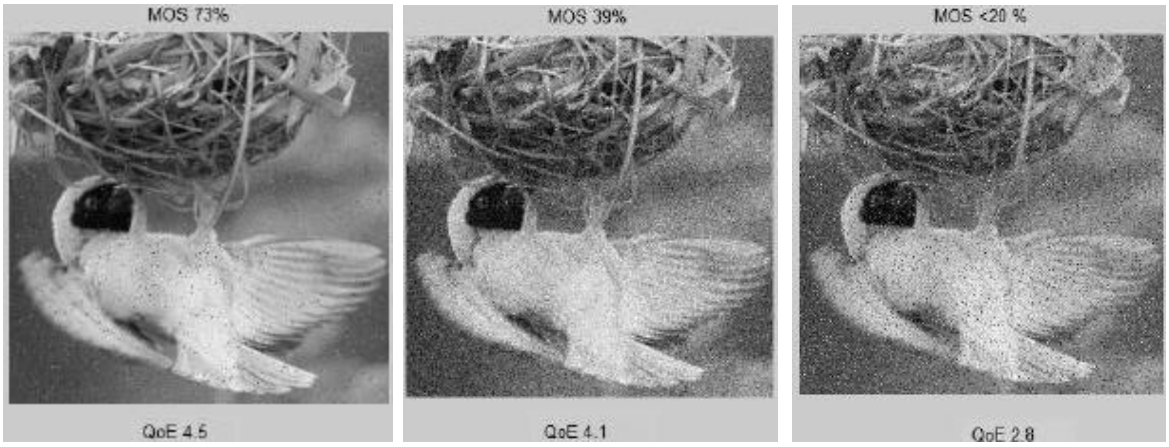

Figure 9. Relationship between MOS and QoE according BER.

The data simulation results are presented in Tables 2 and 3.

Table 2. Original information, which was sent.

#5+BDC123245798BDC123245798BDC123245798zxcvbnm

Table 3. Received data.

BER	MOS	QOE	Received data
$<10^{-2}$	<20	1.3	%»JCtq45718B DÃ527r4° DS1r #2>4792j:cfBnm
$<10^{-6}$	<37	3.6	"5+BEG123"457 9<BDÓ123r4571 YBLC10#245w98 zxcvbnm'
$<10^{-9}$	<92	4.9	#µ+BDC1232457 98BDC12324579 8BDC123245798 zxcfbnm

According to the obtained results in Figure 8 and in Table 3, it is seen, that the higher the error rate du- ring the transmission process, the lower the QoS and QoE parameters for different types of information (in our case for image and data). In this way,

the influence of different intensity fog can cause the vulnerability in Optical Wireless system parameters, but the user can still use the different type of services, just with the different affect to real perceived quality.

6. CONCLUSION

The investigations showed, that using of shorter wavelengths can increase the resilience of OW systems during the fog. Also, it is a big difference in the scale of fog influence to a different type of services, which are transmitted over OW link. If the user receives data, the intensive fog can cause a big impact to the perceived quality of such service. However, if the user is using video service, he can feel just some single failures, but the service will be still in performance. The reason is a lower correlation between MOS and QoE. Due to this, a time interval occurs when the user sees the faults, but the service still can be used, even though that parameters of OW system starts to deteriorate. The main results from these investigations will help in further authors' work by creating a solution for an alert in order to react and prevent service performance degradation under the weather-based disruptions over wireless systems.

ACKNOWLEDGEMENT

This article is based upon work from COST Action CA15127 ("Resilient communication services protecting end-user applications from disaster-based failures — RECODIS") supported by COST (European Cooperation in Science and Technology).

REFERENCES

[1] Majumdar, Arun K., "Advanced Free Space Optics (FSO): A Systems Approach", New York, USA, Spring- er, 2015.

[2] Uysal, M., Capsoni, C., Ghassemlooy, Z., Boucouvalas, A., Udvary, "Optical Wireless Communications: An Emerging Technology", Switzerland, Springer, 2016.

[3] Leitgeb, E., Plank, T., Awan, M.S., Brandl, P., Popoola, W., Ghassemlooy, Z., Ozek, F., Wittig, M., "Analysis and Evaluation of Optimum Wavelengths for Free-Space

Optical Transceivers", in proccedings of 12th Interna- tional Conference on Transparent Optical Networks (ICTON), Munich, Germany, 2010. pp. 1-7.

[4] Leitgeb, E., Bregenzer, J., Gebhart, M., Fasser, P., Merdonig, A., "Free Space Optics – Broadband Wireless Supplement to FiberNetworks", in proccedings of SPIE, Free-Space Laser Communication Technologies XV, vol. 4975, San Jose, CA, 2003. pp. 57-68.

[5] Leitgeb, E., Gebhart M., Sheikh Muhammad, S., Fle- cker, B., Chlestil, C., "Measurement of Light attenuation in dense fog conditions for FSO applications", in pro- ccedings of SPIE, Atmospheric Optical Modeling, Measurement, and Simulation, vol. 5891, Bellingham, WA, 2005. pp. 1-12.

[6] Leitgeb, E., Sheikh Muhammad, S., Flecker, B., Chlestil, C., Gebhart, M., Javornik, T., "The Influence of Dense Fog on Optical Wireless Systems, Analysed by Meas-urements in Graz for Improving the Link-Reliability", in proccedings of 8th International Conference on Transparent Optical Networks (ICTON), Nottingham, United Kingdom, 2006. pp. 154-159.

[7] Leitgeb, E., Birnbacher, U., Kogler, W., Schrotter, P., "High Availability of Hybrid Wireless Networks", in proccedings of SPIE, Reliability of Optical Fiber Components, Devices, Systems, and Networks II, vol. 5465, Bellingham, WA, 2004. pp. 238-249.

[8] Nur Islam, Nur Al Safa Bhuiyan. Effect of operating wavelengths and different weather conditions on performance of point-to-point free space optical link. Inter-national Journal of Computer Networks & Communications (IJCNC) Vol.8, No.2, March 2016.

[9] Aderemi A. Atayero, Oleg I. Sheluhin and Yury A. Ivanov. Modeling, Simulation and Analysis of Video Streaming Errors in Wireless Wideband Access Net- works. Springer. 2013.

MULTIFUNCTIONAL ADAPTIVE SYSTEM FOR PHYSIOTHERAPY (selected from CEMA'17 Conference)

Atanas Dimitrov, Sasho Guergov, Dimiter Tz. Dimitrov

Technical University of Sofia,

8, Kliment Ohridsky Str., 1000, Sofia, Bulgaria

Abstract

An investigation on structure of one multifunctional adaptive system for physiotherapy with measurement devices has been done in the paper. In the paper there are descriptions of different parts of the multifunctional system. Some characteristics and properties of different units of multifunctional system have been done, also. Some possibilities for simultaneously applications of different system's units are described, also. It's important to provide simultaneously application of different system's units only when their physiological influences on the human body are compatible. Simultaneously application of magneto-therapy, mechanical acupressure and cranial electro stimulation are described in the paper.

1. INTRODUCTION

There are many well know methods for physiotherapy, which can be applied in different cases of pathology. Often according to these methods there is a separate "hard" application of different external influences one by one. One new tendency in medicine is connected with application of multifunctional adaptive systems for physiotherapy. These systems can provide not only separate influence of different external influences, but simultaneously influence of these external influences of on one or on different part of the human body. Sometimes a physical interaction between these external influences can be seen as in the case of simultaneously influence of low frequency electrical and magnetic fields. In other cases, there is no formal physical interaction between external influences, but there is physiological interaction as in the cases of simultaneously influence of low frequency magnetic field and acupressure or acupressure and Cranial Electrotherapy Stimulation (CES). CES is the application of low-level pulsed electrical currents (usually less than 1mA) applied to the head for medical and/or psychological purposes. It would be very convenient for physicians if much more units for different external influences

would be available as parts of one multi- functional adaptive system for physiotherapy. For instance, this system can provide influence of low frequency magnetic field, low frequency electrical field (including Cranial Electrotherapy Stimulation) and acupressure.

2. DESIGN OF DEVICES FOR CREATING LOW FREQ. MAGNETIC FIELD

The application of China's method for acupressure is very actual in medical therapy, now. Usually a physician provides application of acupressure by his hands. It's inconvenient first of all for the physician. He's able to work for a short time. Then he can continue after relax, but the number of these procedures per day are limited. In other side it would be better to provide acupressure simultaneously on more points on the human body. However, this is impossible because the physician has only two hands.

The results of therapy by acupressure would be better if there would be provided more intensive movement of the blud in around the points of acupressure. This activation of blud's movement can be provided by application of low frequency magnetic field together with acupressure.

It's clear that it' s necessary to provide special device for acupressure, which can be used together with special device for creating of low frequency magnetic field around the points for acupressure. Therefore, the application of system for simultaneously application of acupressure and low frequency magnetic field is very actual, now.

Usually the low frequency magnetic field can be created using two coils, connected to the output of apparatus for magneto-therapy. This apparatus is a source of special electrical signals for the coils.

Often the application of above described method for therapy is on the hand because there are situated many points of acupunctures.

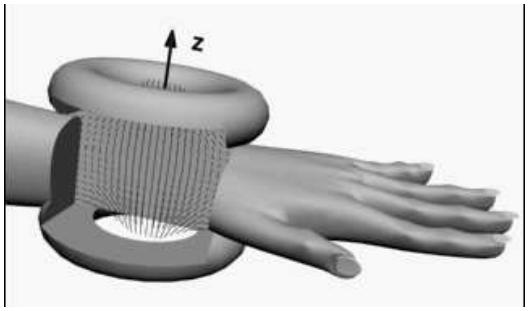

Figure 1. A possibility for disposition of two coils on the hand

The space configuration of the lines of vector of magnetic induction can be seen on Fig. 1. It's well known that on the spine there are many points of acupuncture, also. Some examples for disposition of coils on the spine can be seen on Fig. 2. The axis of space components of magnetic induction of magnetic field, created by different coils can be seen on Fig. 2, also. A girdle coil (Fig.3) can be used for magnetotherapy, also.

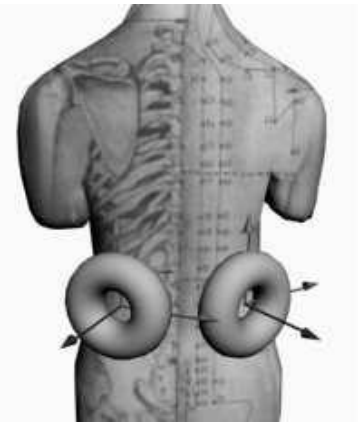

Figure 2. Some examples for disposition of coils on the spine.

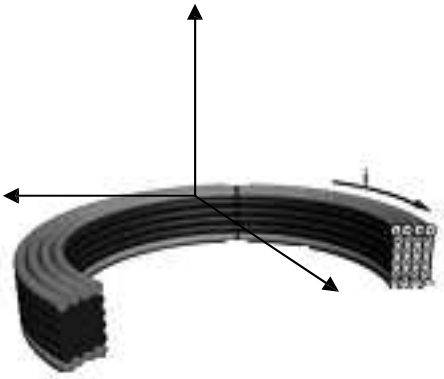

Figure 3. A girdle coil.

3. MEASUREMENT OF PARAMETERS OF LOW FREQ. MAGNETIC FIELD

First of all, it's important to provide measurement of the value of magnetic induction in the process of magnetotherapy. The sensor has been putted in different points around the girdle coil. The measurement of the gidle coil's current has been done by ordinary ampermeter. The measurement of module of magnetic induction on the axes X and Z (Fig.3) has been done. The results of experimental measurements together with the results of calculation of the module of magnetic induction on axes X and Z can be seen on Fig. 4. and Fig.5 respectively.

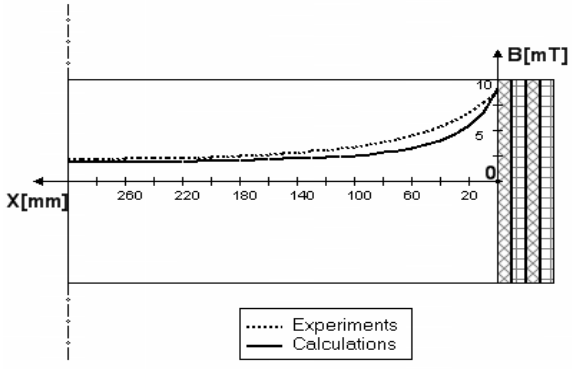

Figure 4. Module of magnetic induction on the axis X.

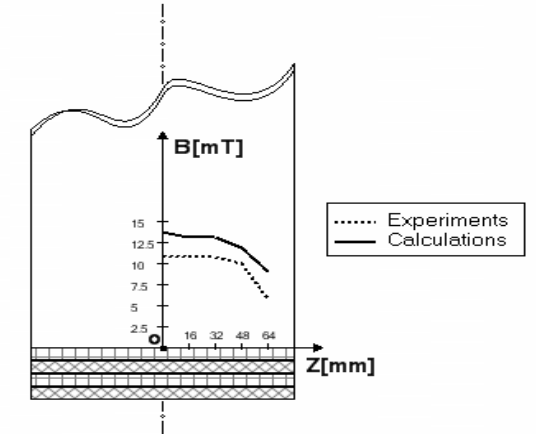

Figure 5. Module of magnetic induction on the axis Z.

4. LEVEL OF ERRORS OF MEASUREMENT OF THE VALUE OF MAGNETIC INDUCTION

The main causes for errors between calculated and measurement results are: the finite sizes of the sensor. The results of calculation and results of experimental measurements are similar. It was the main goal of investigation. Of course, it's possible to obtain more precise methods and measurement devices, but it's not necessary in the case of magnetotherapy, where usually the values of magnetic in- duction are 10-30 mT and 10% error is acceptable. It's clear that only one small translation of the hu- man body in the girdle coil would be enough for an error of the value of module of magnetic induction in an arbitrary point of the human body, more than 10%. The value of relative magnetic permeability of live tissue is $\mu_r \approx 1$ as in the air.

Therefore, computer simulation can be used successfully for future investigation of space configuration of low-frequency magnetic field in the human body, also. This is the main conclusion of the above investigations.

5. DESIGN OF DEVICES FOR CREATING OF CRANIAL ELECTROTHERAPY STIMULATION

Often, in the last time there is application of therapy by acupressure simultaneously with electrotherapy especially with Cranial Electrotherapy Stimulation. Usually physician provide application of acupressure by his hands and he should be very careful be- cause this therapy is on head. Of course, it's possible to be used separately one by one both therapy by acupressure and Cranial Electrotherapy Stimulation, but the effect of therapy especially effect of re- laxation would be more good in the case of simultaneously application.

Sometimes in the cases of high values of the blood pressure, stress and loss of the sleep physicians use successfully a unit for magneto-therapy for de- creasing of blood pressure and Cranial Electrotherapy Stimulation for sleeping using another unit for electro-seeping. In the last time often physicians use both magnetotherapy and electro-sleeping simultaneously. This allow them to obtain more good effect of therapy. The method of Cranial Electrotherapy Stimulation is new one since the end of last century. Therefore, some preliminary separate investigation of this method has been done before

simultaneously application of the method together with magnetotherapy or/and acupressure.

CES treatment may result indirectly in increased blood flow to the brain. Hence its possible contra- indication in recent hemorrhagic stroke patients. This same effect can cause brief increased blood flow beneath the electrodes behind the ears. This red- ness should not be cause for concern. This is an extremely rare occurrence. Cranial electrotherapy stimulation devices are generally similar in size and appearance to standard transcutaneous electrical nerve stimulators (TENS), but produce very differ- rent waveforms. Standard milliampere-current TENS devices must never be applied transcranially. CES electrodes can be placed bitemporally, bilaterally in the hollow behind the ears just anterior to the mas- toid processes, or clipped to the earlobes. This depends on the device being used. Most CES devices should produce a pulse repetition rate (PRR) of 100 Hz. Some produce a PRR as low as 0.5, or as high as 15,000 Hz. Most CES units are user friendly. After having put on either the electrodes or the ear-clips and inserted the lead wire into the jack, it's all very simple. CES units either feature an on-off knob that also controls the amplitude (turning it to the right increases the amount of current) as in the 100 Hz devices. A CES generates an adjustable current of 80 to 600 μA that flows through clips placed on the earlobes. The waveform of this device is a 400 milliseconds positive pulse followed by a negative one of the same duration, then a pause of 1.2 seconds. The main frequency is 0.5 Hz, i.e., a double pulse every 2 seconds. Current output is limited to 600 μA max and can be regulated from 80 to 600μA. A LED can flashe every 2 seconds signaling proper operation and can also be used for setting purposes.

A common CES configuration is 100 Hz with a maximum current output of 1.5 mA, current amplitude similar to that in the human body. A device of CES as part of multifunctional system for physiotherapy can be seen on Fig. 6.

Figure 6. Device for Cranial Electrostimulation

5. DESIGN OF MECHANICAL DEVICE FOR ACUPRESSURE

The design of mechanical devices for acupressure should be connected with design of coils for magnetotherapy as the multifunctional system should provide simultaneously application of acupressure and magneto-therapy. It's well known that the magnetic field can increase the velocity of ions of blood. Because of that the effect of acupressure can be more good. Usually the line of mechanical pressure is the axis of coils. The sizes of coils can be different ac- cording to the sizes of "active" area around of the acupuncture points.

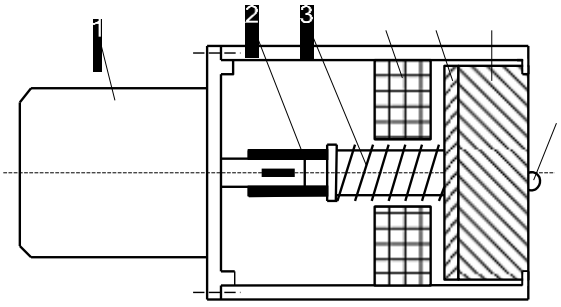

Figure 7. Mechanical device for acupressure

On Fig. 7 a mechanical device for acupressure is shown, where:

1 – motor;
2 – axle;
3 – shaft;
4 – a coil, which provides axial movement of the shaft;
5 – metal disk;
6 – plastics body;
7 – massage pimple (osezatel).

The modified device for acupressure simultaneously with low frequency magnetic field can be seen on Fig. 8. It can be seen that the shaft is in the coil for magnetotherapy.

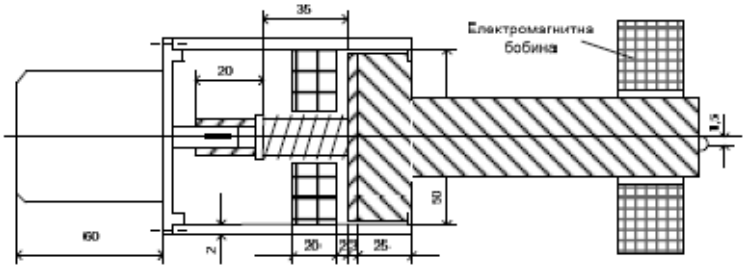

Figure 8. Modified mechanical device for acupressure simultaneously with application of low frequency magnetic field.

5. CONCLUSION

1. It's clear that the process of physiotherapy can be more effective in the case of simultaneously application of several unites (apparatuses or/and devices) for different physical influences on the human body than separate application of these unites one by one.

2. The big advantage of one multifunctional system for physiotherapy is that it's flexible and user friendly. Therefore, it's easy to be obtained different configuration of system and to provide applications of many methods for physiotherapy. Because of that the system is adaptive to medical methods for therapy.

3. Usually every multifunctional system can be developed easy. It's enough to add new units which should be compatible with the rest system's units.

REFERENCES

[1] Kirsch, D.L. and Smith, R.B., "The use of cranial electrotherapy stimulation in the management of chronic pain: A review", NeuroRehabilitation 14 (2000) p.85-94.

[2] Winick, R.L., "Cranial electrotherapy stimulation (CES): a safe and effective low cost means of anxiety control in a dental practice", Gen. Dent. 47 (1999) p. 50-55.

[3] Lichtbroun, A.S., Raicer, M.C. and Smith R.B., "The treatment of fibromyalgia with cranial electrotherapy stimulation", J. Clin. Rheumatol. 7 (2001) p.72-78.

[4] Hozumi, S, Hori, H, Okawa, M, Hishikawa, Y and Sato, K., "Favorable effect of transcranial electrostimulation on behavior disorders in elderly patients with dementia: a double-blind study", Inter. J. Neurosci. 88 (1996) p.1-10.

[5] Southworth, S., "A study of the effects of cranial electrical stimulation on attention and concentration", Tntegr. Physiol. Behav. Sci. 34 (1999) p.43-53.

[6] Schroeder, M.J. and Barr R.E., "Quantitative analysis of the electroencephalogram during cranial electrotherapy stimulation", Clin. Neurophysiol. 112 (2001) p. 2075-2083.